Polyhedron 171 (2019) 32–40

Contents lists available at ScienceDirect

Polyhedron

journal homepage: www.elsevier.com/locate/poly

Creation of controllable cationic and anionic defects in tunnel manganese oxide nanowires for enhanced oxygen evolution reaction

Patrick J. West, Bryan W. Byles, Ekaterina Pomerantseva *

Materials Electrochemistry Laboratory, Department of Materials Science and Engineering, Drexel University, Philadelphia, PA 19104, USA

ARTICLE INFO

Article history:
Received 7 April 2019
Accepted 26 June 2019
Available online 9 July 2019

Keywords:
Tunnel manganese oxide nanowires
Alpha-MnO_2
Oxygen evolution reaction (OER)
Oxygen vacancies
Cobalt doping

ABSTRACT

The development of efficient oxygen evolution reaction (OER) catalysts is crucial to the environmental and economic feasibility of electrolysis for the production of hydrogen gas. In this work, two facile chemical treatments, acid leaching and transition metal doping, were shown to modify the chemical and structural properties of low cost and environmentally friendly α-MnO_2 nanowire catalysts resulting in increased OER activity. Through a combination of XPS and XRD analyses, it was shown that a molten salt treatment of α-MnO_2 nanowires with $Co(NO_3)_2$ introduced Co^{2+} ions into the structural tunnels. The introduction of minimal amounts of cobalt (<6 at. %) more than doubled ultimate current densities achieved in linear sweep voltammetry tests. This result was attributed to a reduction of the average oxidation state of manganese in Co-doped samples and a decrease in Tafel slope below 80 $mV{\cdot}dec^{-1}$. Acid leaching, on the other hand, is believed to modify nanowire topography through the creation of oxygen and manganese vacancies, exposing more active sites to participate in catalysis. A characterization approach combining atomic absorption spectroscopy and iodometric titration revealed a 5.1% increase in oxygen vacancies after 72 h of interaction with nitric acid. When these controllable defect formation approaches were applied in tandem, the high activity of the cobalt-doped samples was combined with the increased number of exposed active sites achieved through acid leaching producing a highly efficient electrocatalyst with more than a 3-fold increase in OER activity over pristine α-MnO_2 nanowires. Our results establish that scalable and easy-to-implement approaches, such as acid leaching and transition metal doping, can lead to more than a three-fold increase in OER activity of low-cost non-toxic manganese oxides. This methodology can be beneficial for other material systems used as OER electrocatalysts.

1. Introduction

As of 2010, the majority of hydrogen in the United States is produced via the reformation of methane gas and water vapor, which results in carbon monoxide and hydrogen gas [1]. The potential for a more environmentally conscious method for hydrogen production exists in the two-step electrolysis process, wherein water is split into hydrogen and oxygen gases via the application of a direct current. Electrolysis is a carbon free method to produce hydrogen that does not result in the formation of harmful greenhouse gases, and electrolysis coupled with renewably sourced electricity from solar cell or wind is an attractive alternative to current hydrogen production methods [1]. The anodic half reaction of electrolysis, the oxygen evolution reaction (OER, Eq. (1)), is a four-electron process with higher voltage requirements and slower kinetics than the cathodic hydrogen evolution reaction (HER, Eq. (2)) causing OER to be the major hurdle in achieving high efficiency hydrogen production via electrocatalysis [2].

$$2H_2O_{(l)} \rightarrow O_{2(g)} + 4H^+ + 4e^- \quad (1)$$

$$2H^+ + 2e^- \rightarrow H_{2(g)} \quad (2)$$

Precious metal oxides, such as RuO_2 and IrO_2, have been investigated as catalysts to reduce the overpotential in OER and have demonstrated excellent initial catalytic activity, but readily oxidized into RuO_4 and IrO_3 in alkaline solutions [2,3]. Moreover, their high cost has prompted extensive research into alternative and more affordable OER catalysts, bringing period 4 transition metal (Mn, Fe, Co, and Ni) oxides to the forefront of investigation [4]. Manganese oxides are particularly promising as OER catalysts due to their stability in aqueous alkaline environments and versatility of crystal structures and morphologies, uniquely characteristic of this

* Corresponding author.
E-mail address: ep423@drexel.edu (E. Pomerantseva).

https://doi.org/10.1016/j.poly.2019.06.050
0277-5387/

family of materials [2,5]. These properties combined with ease of production, low cost, and environmental friendliness make manganese oxides attractive candidates for further exploration [6,7].

Comparative studies of several MnO_2 polymorphs carried out by the Stahl group and the Suib group, suggest that α-MnO_2, also known as hollandite-type manganese oxide, is the most catalytically active manganese oxide crystal structure in OER in alkaline environments [8–10]. Additionally, the one-dimensional nanowire morphology attainable by α-MnO_2 have been shown to be more active towards OER catalysis compared to lower surface area particles, such as platelets or nanosheets [7]. Therefore, α-MnO_2 nanowires are a promising manganese oxide for further modification with the aim of enhancing electrocatalytic performance.

The crystal structure of the α-MnO_2 phase (space group $I4/m$), is composed of corner and edge sharing MnO_6 octahedra arranged in tunnels around stabilizing ions and water molecules (Fig. 1). Here we focused on K^+ ion stabilized α-MnO_2 with a chemical composition of $K_\beta MnO_2$ and commonly reported β values of 0.11 [11]. At the same time, α-MnO_2 polymorphs with the β values reaching as high as 0.75 are known as well [12]. The ionic content within these structural tunnels results in a mixed $Mn^{3+/4+}$ oxidation state of manganese ions. Much work has been done to manipulate the average oxidation state of Mn to be more favorable to OER activity in various manganese oxides [8,9], with common approaches involving nanoparticle decoration [13], the introduction of catalytically active species like Co [14] or Ni [15] into layered phases, and the introduction of cation and anion point defects [16].

In this work, we expanded on this progress by providing a facile and tunable route for the introduction of cobalt dopant ions into the structural tunnels of α-MnO_2 nanowires. Additionally, acid leaching, a powerful technique previously shown to partially remove stabilizing ions in tunnel manganese oxides [12,16–19], affect the oxidation state of manganese in structural tunnels and create oxygen vacancies through a Mn^{3+} ion disproportionation mechanism [16], was explored to improve the catalytic activity towards OER. Following trends identified elsewhere [6], the chemical and structural changes introduced via interactions with nitric acid and cobalt nitrate, both independently and in tandem, were shown to greatly improve the OER catalytic activity of α-MnO_2 nanowires, attributed to the creation of defect-rich mixed component systems. Moreover, the tunable nature of these treatments allows for precise control over the anion and cation sublattices of manganese oxides in a way that has not been utilized in past to enhance the catalytic activity of the sample for electrochemical water splitting applications.

2. Experimental

2.1. Synthesis and chemical modification of α-MnO_2 nanowires

α-MnO_2 nanowires were prepared following a procedure reported by Gao et al. [20] 316 mg of $KMnO_4$ (Acros Organics) and 108 mg of dehydrated NH_4Cl (Stream Chemicals) were dissolved in 100 mL of deionized H_2O. The solution was stirred until complete dissolution of the precursors, and then aliquots of 20 mL were added to 23 mL Teflon™ autoclaves (Parr Instruments). The autoclaves were heated at 150 °C for 50 h. The formed solid product was thoroughly washed and dried at 100 °C for 12 h.

Acid leaching was performed by adding 300 mg of pristine powder to 100 mL of 16 M HNO_3 solution (Fischer Scientific, 70% by volume). The material was stirred in the acid solution at medium speed for 72 h [17]. Samples were then filtered out of the solution and thoroughly washed with DI water until neutral pH via vacuum filtration. Typically, 300 mL of DI water per 100 mg of material was added in aliquots of 100 mL. Samples were then dried at 100 °C for 12 h in an oven.

In a typical cobalt doping experiment, 5 g of $Co(NO_3)_2{\cdot}6H_2O$ (Acros Organics) was placed in a 23 mL Teflon™ liners (Parr Instruments) and heated on a stir plate until $Co(NO_3)_2{\cdot}6H_2O$ melted (T_m = 55 °C) forming an aqueous solution of cobalt nitrate. This step was followed by dispersing 20 mg of pristine α-MnO_2 or acid leached α-MnO_2 (AL α-MnO_2) nanowires in 5 mL of formed warm $Co(NO_3)_2{\cdot}$solution, placing Teflon™ liners containing the dispersion

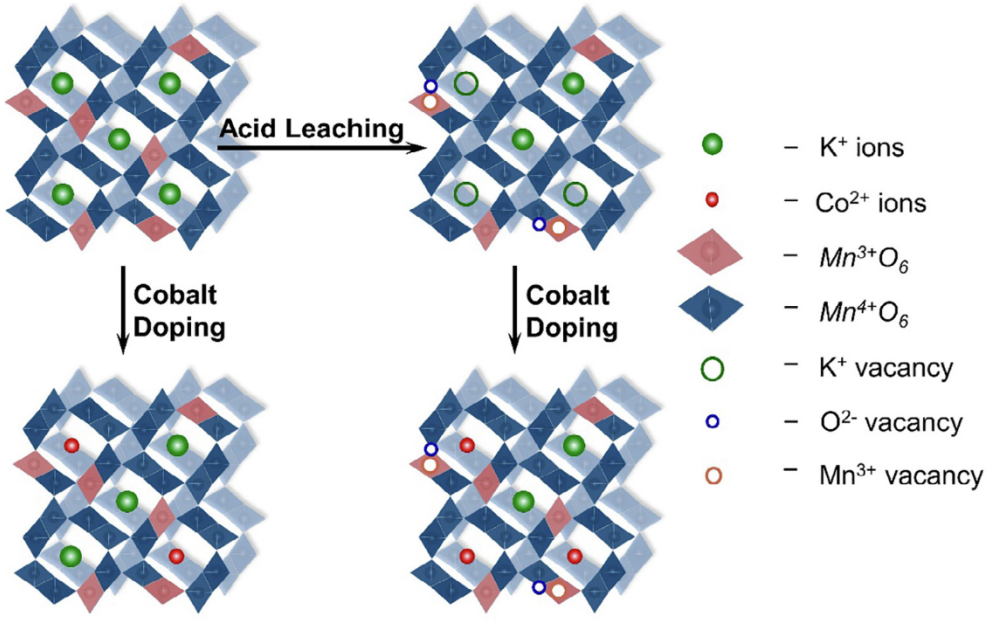

Fig. 1. Schematic illustration of the chemical modification approaches explored in this work with the aim to enhance catalytic activity of α-MnO_2 nanowires in OER. Acid leaching was carried out at room temperature in concentrated nitric acid. Cobalt doping was achieved by holding α-MnO_2 nanowires in $Co(NO_3)_2$ melt at 120 °C. Defect-rich α-MnO_2 nanowires, combining modifications in both anionic and cationic sublattices, were obtained by first reacting pristine nanowires with nitric acid and then with the cobalt nitrate melt.

into stainless steel autoclaves and heating them at various temperatures (80°, 100°, and 120 °C) for 8 h. The obtained powder was filtered, thoroughly washed with DI water, and dried at 100 °C for 12 h in an oven.

2.2. Material characterization

Phase composition was identified utilizing X-ray powder diffraction (XRD) with a Rigaku SmartLab X-Ray diffractometer (Japan) using Cu Kα radiation and a step size of 0.02° 2θ. Sample morphology was characterized using a Zeiss Supra 50VP (Germany) scanning electron microscope (SEM) with an energy dispersive X-ray (EDX) spectroscopy attachment. The K:Mn ratio in the chemical composition of materials was determined by EDX and verified with atomic absorption spectroscopy (AAS). AAS tests were performed using a Varian 240FS flame atomic absorption spectrometer (Agilent Technologies) with an air-acetylene flame and single-element hollow cathode lamps. For AAS testing, samples were prepared by dissolving 10 mg of manganese oxide in a 5% HNO_3 and 3% H_2O_2 solution. Thermal stability of acid leached samples was evaluated via thermogravimetric analysis (TGA) using a TA Instruments Thermogravimetric Q50 Analyzer, with a ramp rate of 10 °C minute^{-1} from room temperature to 1000 °C under argon gas. Average oxidation states of manganese, cobalt and oxygen were determined through X-ray photoelectron spectroscopy (XPS, Physical Electronics VersaProbe 5000).

2.3. Iodometric titration

An iodometric titration (IT) method adapted from reports by Laiho et al. [21] and Vazquez-Vazquez et al. [22] was used to assess the average oxidation state (AOS) of Mn in the pristine and acid-leached α-MnO_2 nanowires. A known amount of ground nanowires was dissolved in a solution of excess KI and HCl. The chlorine ions reduce manganese producing Mn^{2+} ions and Cl_2 (Eqs. (3) and (4)); the latter reduces I^- to I_2 (Eq. (5)), which is accompanied by a change of the solution color to umber. This solution was then titrated until clear using $Na_2S_2O_3$ (Eq. (6)):

$$2Mn^{III} + 2Cl^- \rightarrow Cl_2 + 2Mn^{II} \quad (3)$$

$$Mn^{IV} + 2Cl^- \rightarrow Cl_2 + Mn^{II} \quad (4)$$

$$Cl_2 + 2I^- \rightarrow 2Cl^- + I_2 \quad (5)$$

$$2S_2O_3^{2-} + I_2 \rightarrow 2I^- + S_4O_6^{2-} \quad (6)$$

The chemical formula of α-MnO_2 (or more accurately, $K_{0.15}MnO_2$) can be rewritten as $K_{0.15}Mn^{III}_{1-\alpha}Mn^{IV}_{\alpha}O_2$ and through stoichiometry α is found by Eq. (7):

$$\alpha = \frac{V * n * M}{m} - 1 \quad (7)$$

where V is the volume of $S_2O_3^{2-}$ solution titrated, n is the normality of the of the $S_2O_3^{2-}$ solution (in this case 0.2 N), M is the molar mass of the sample and m is the mass of the sample. α, as found via iodometric titration, can also be expressed as the ratio of Mn^{4+} to the total amount of Mn and can quickly be found by subtracting 3 from the average oxidation state. More details on using this approach for determining chemical composition of pristine and acid-leached α-MnO_2 nanowires are given in Supporting Information (Appendix A). This technique however cannot be used for the Co-doped α-MnO_2 nanowires, because of the side reactions that are known to occur between cobalt ions and chlorine.

2.4. Electrochemical characterization

The OER performance of the pristine and chemically modified α-MnO_2 nanowires was evaluated using a Pine Research Instrumentation Modulated Speed Rotator (MSP). Working electrodes were fabricated via drop-casting of inks composed of a 1:1 ratio of active material to carbon black (Alfa Aesar) in 45 μL Nafion® binder (Ion Power) and 350 μL ethanol onto a glassy carbon working electrode (mass loading 0.25 mg/cm^2 of active material). Linear Sweep Voltammetry (LSV) experiments were carried out at 1600 RPM in 0.1 M KOH (Sigma Aldrich) electrolyte over a voltage window of 1.0–1.85 V vs RHE. The tests were performed with a graphite counter electrode and a Ag/AgCl reference electrode (CH Instruments, Inc.).

3. Results and discussion

3.1. Acid leaching and cobalt doping

The morphology and structure of pristine and chemically modified α-MnO_2 nanowires were characterized using SEM and XRD analysis, respectively (Fig. 2). The XRD patterns of all four synthesized materials were indexed to JCDPS file #44-014 and indicated that no impurities were detected (Fig. 2a). Comparing the XRD patterns of pristine and acid-leached α-MnO_2 nanowires shows a shift to a higher 2θ values for all reflections after interaction with nitric acid (Fig. 2a, b). This shift was attributed to a contraction of the lattice due to the removal of stabilizing K^+ ions from the structural tunnels of α-MnO_2, as confirmed by EDX spectroscopy and AAS (Tables 1 and Table S1 in Supporting Information). By varying the time of interaction between nanowires and concentrated nitric acid, it was found that the maximum time that does not lead to the phase transformation was ~72 h (Supporting Information, Table S1). Therefore, these conditions were used to obtain acid-leached α-MnO_2 nanowires throughout this work, labeled as 72 h AL α-MnO_2. Unit cell parameters determined using Rietveld refinement showed a decrease in the unit cell parameter a from 9.832 (5) Å to 9.761(4) Å after acid leaching (Supporting Information, Table S2). The unit cell parameter c of the tetragonal unit cell, however, remained relatively unchanged at 2.852(2) Å, showing that the unit cell contraction occurs mainly in the a-b plane, or across the face of the tunnels. This decrease in unit cell parameter a and the removal of K^+ ions suggest a H^+–K^+ ion exchange, consistent with previous reports on acid leaching of tunnel manganese oxides, like α-MnO_2 [18].

Cobalt doping was carried out at three temperatures (80, 100, and 120 °C) for 8 h. Interaction of α-MnO_2 nanowires with the cobalt nitrate melt at temperatures higher than 120 °C and durations longer than 8 h failed to preserve one-dimensional morphology of the particles and were not further investigated. Cobalt doping allowed for the introduction of cobalt ions into the α-MnO_2 crystal structure. AAS analysis revealed that cobalt content increased linearly with temperature to form $Co_{0.02}MnO_2$, $Co_{0.03}$-MnO_2, and $Co_{0.04}MnO_2$, for annealing performed at 80, 100, and 120 °C, respectively. Rietveld refinement of the XRD patterns (Fig. 2a, b) revealed that in case of $Co_{0.04}MnO_2$ the unit cell parameter a decreased from 9.832(2) Å to 9.817(3) Å, but the c parameters remained relatively constant at 2.849(3) Å and 2.855(05) Å for pristine and cobalt-doped materials, respectively (Table S2). Under the same synthesis conditions at 120 °C for 8 h in $Co(NO_3)_2$ melt, the acid-leached sample allowed for a higher amount of intercalated cobalt, forming a material with the chemical formula of α-$Co_{0.06}MnO_2$, which is largely attributed to the lower K^+ ion content and a more open crystal structure in defect rich acid-leached samples allowing for cobalt ions to be more readily incorporated into

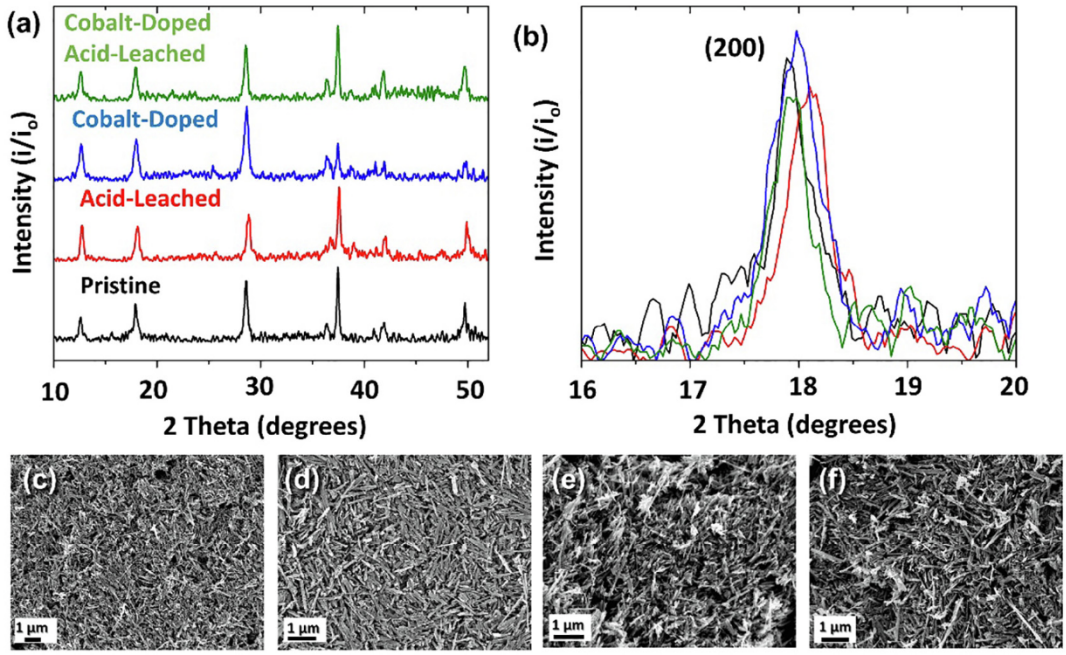

Fig. 2. Structure and morphology characterization of α-MnO_2 nanowires in the pristine and chemically modified forms. (a) XRD patterns and (b) a close-up view of the (2 0 0) reflection in XRD patterns of the pristine, acid-leached, Co-doped, and Co-doped acid-leached α-MnO_2 nanowires. (c–f) SEM images of the ground (c) pristine, (d) acid-leached, (e) Co-doped, and (f) Co-doped acid-leached α-MnO_2 nanowires.

Table 1
Synthesis conditions and chemical composition of pristine and chemically modified α-MnO_2 nanowires.

Sample name	Synthesis conditions	Chemical composition
Pristine α-MnO_2	Hydrothermal treatment at 150 °C for 50 h	$K_{0.15}MnO_{1.96}$
72 h AL α-MnO_2	Chemical wet mixing at room temperature for 72 h	$H_{0.12}K_{0.03}Mn_{0.90}O_{1.86}$
α-$Co_{0.02}MnO_2$	Molten salt treatment at 100 °C for 8 h	$Co_{0.02}K_{0.04}MnO_{2-\delta}$
α-$Co_{0.04}MnO_2$	Molten salt treatment at 120 °C for 8 h	$Co_{0.04}K_{0.09}MnO_{2-\delta}$
72 h AL α-$Co_{0.03}MnO_2$	Chemical wet mixing at room temperature for 72 h then molten salt treatment at 100 °C for 8 h	$Co_{0.03}K_{0.03}Mn_{0.9}O_{2-\delta}$
72 h AL α-$Co_{0.06}MnO_2$	Chemical wet mixing at room temperature for 72 h then molten salt treatment at 120 °C for 8 h	$Co_{0.06}K_{0.03}Mn_{0.9}O_{2-\delta}$

the crystal lattice. The higher fraction of chemically doped cobalt ions in the acid-leached α-MnO_2 nanowires expanded structural tunnels with the unit cell parameter *a* of α-$Co_{0.06}MnO_2$ increasing to 9.849(3) Å without much effect on the unit cell parameter *c* (Table S2).

SEM images in Fig. 2c–f, reveal that the one-dimensional morphology of the pristine α-MnO_2 is preserved under the selected conditions used in the chemical modification processes. Table 2 shows sample names used in this work and summarizes synthesis conditions. The chemical compositions in Table 2 were determined via combined AAS and IT characterization methodology, discussed in detail below.

Table 2
Average oxidation state and chemical ratio of pristine and acid leached α-MnO_2 compositional constituents. Average oxidation state of Mn and K:Mn ratio were found using IT and AAS, respectively. Values taken as constants are given in black, values found experimentally are given in red, values calculated from Mn disproportionation are given in green, and values calculated from charge balancing are given in blue.

	Cation			Anion
Sample	H^+	K^+	Mn^{x+}	O^{2-}
Pristine α-MnO_2	+1(0)	+1(0.15)	+3.774(1)	-2(1.96)
72 hour acid-leached α-MnO_2	+1(0.127)	+1(0.027)	+3.966(0.898)	-2(1.858)

3.2. Oxygen vacancy characterization

To gauge the significance and quantify the formation of oxygen vacancies in 72 h acid-leached α-MnO_2 nanowires, thermogravimetric analysis (TGA) combined with XRD analysis was used to understand weight loss during heat induced phase changes (Fig. 3a–c). It is believed that in an inert environment, weight loss during phase change will be largely due to evolving oxygen and that the acid-leached samples will undergo less weight loss because they are more oxygen deficient. However, TGA testing in an inert atmosphere revealed that an acid-leached material lost more mass than the pristine α-MnO_2 nanowires in a similar temperature range (Fig. 3a). To explore this finding further, samples were annealed at 675 °C and 850 °C for two hours. These temperatures were chosen to fall between the bimodal weight loss exhibited by acid-leached samples (Fig. 3a). SEM images of annealed materials showed that the one-dimensional nanowire morphology of pristine nanowires is preserved at higher temperatures than that of the acid-leached material (Fig. 3d–i) agreeing with the lower thermal stability of the acid-leached material, revealed by TGA. This finding was attributed to the increased concentration of point defects and supports the rapid mass loss exhibited by the acid-leached material. SEM images of the annealed samples demonstrated the formation of particles with platelet morphology indicative of phase transformations occurring with the materials (Fig. 3f and i).

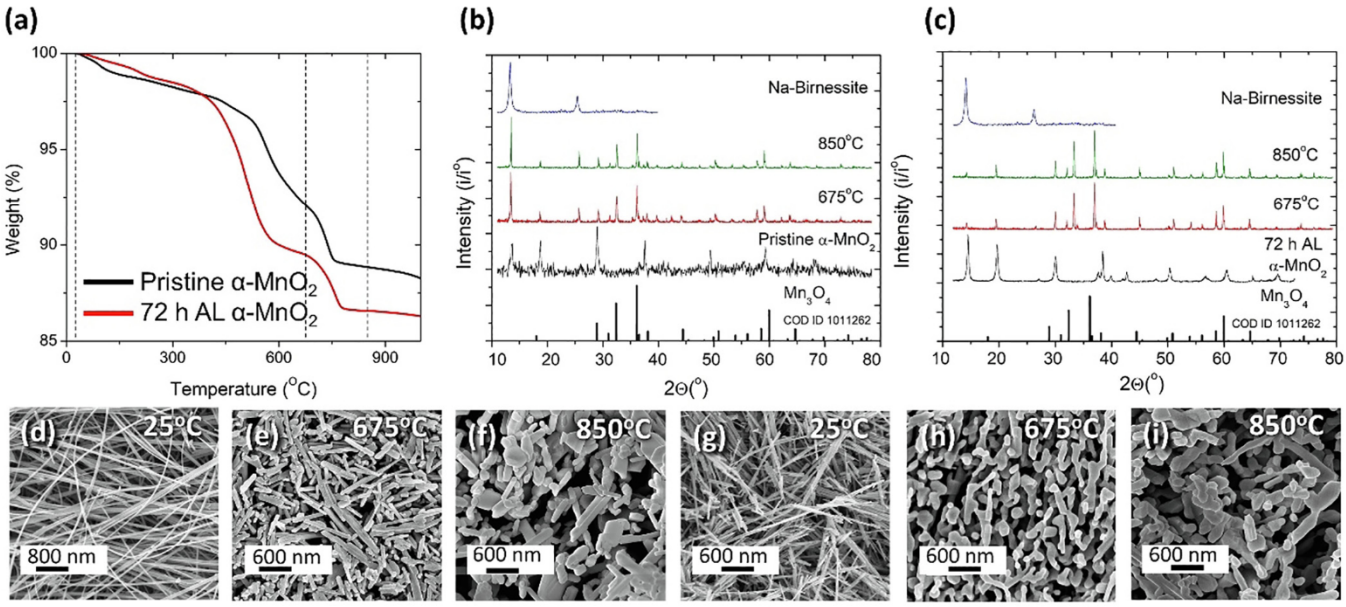

Fig. 3. Annealing induced phase transformation of the pristine and acid-leached α-MnO_2 nanowires. Acid-leached nanowires were obtained via interaction with concentrated HNO_3 for 72 h at room temperature. (a) TGA curves of pristine and acid-leached α-MnO_2 nanowires. (b and c) XRD patterns of (b) pristine and (c) acid-leached nanowires annealed at 675 and 850 °C as compared to non-annealed nanowires. XRD data of Mn_3O_4 and Na-birnessite phases are shown for reference. (d–i) SEM images of (d–f) pristine and (g–i) acid-leached α-MnO_2 nanowires before annealing and after annealing at 675 and 850 °C. All annealing experiments were carried out in the inert atmosphere to prevent oxidation.

The annealing study showed that after annealing at 850 °C both pristine and acid-leached α-MnO_2 nanowires formed a hausmannite Mn_3O_4 phase (Fig. 3b and c). However detailed analysis of the XRD patterns revealed a significant difference in phase evolution of pristine and acid-leached α-MnO_2 nanowires at high temperatures. Two peaks at 11 and 16° 2θ were present in the XRD pattern of pristine material after annealing at 850 °C and absent in the XRD pattern of the annealed acid-leached nanowires. These peaks were phase matched to the layered MnO_2 birnessite phase, which can be stabilized by Na^+ or K^+ ions in the interlayer region, suggesting that birnessite–MnO_2 can only form with excess oxygen available in the pristine α-MnO_2, but not in the oxygen deficient acid-leached α-MnO_2. Formation of the layered birnessite phase would cause oxygen to remain within the structure resulting in less overall weight loss. This phenomenon is believed to account for the thermal stability behavior exhibited by the pristine and acid-leached α-MnO_2 nanowires.

To take this one step further, thermogravimetric-mass spectroscopy (TGA-MS) analysis was used to give insight into what species were evolving at each region of weight loss (Supporting Information, Fig. S1). The acid-leached materials first evolved O_2 gas at 500 °C, as compared to 575 °C in case of the pristine material, supporting that the acid-leached material more rapidly degrades. Additionally, acid-leached samples were shown to evolve mainly oxygen or hydrogen containing OH^- groups. This agrees with the XPS analysis that shows evidence of more Mn-OH groups on the surface of the acid-leached samples (Table 3) and the theory of the K^+–H^+ exchange mechanism that introduces protons into the crystal structure in the form of the hydroxyl groups. The TGA–MS study further reinforces the validity of formation of oxygen vacancies during acid leaching of α-MnO_2.

While the TGA study corroborated the idea that the acid-leached samples were oxygen deficient, it did not provide a pathway to determine the amount of oxygen vacancies formed during acid leaching. To evaluate the fraction of oxygen vacancies in the structure of pristine and acid-leached α-MnO_2 nanowires, a combined atomic absorption spectroscopy and iodometric titration (AAS/IT) approach was developed. The AAS/IT approach is discussed in detail in Supporting Information, Appendix A. The characterization of the pristine nanowires was rather straightforward: AAS measurements established the K:Mn ratio, and IT was used to determine the average oxidation state (AOS) of Mn. Then charge balance principle was applied, resulting in the chemical formula of $K^+_{0.15}Mn^{3.77+}_1O^{2-}_{1.96}$ for pristine α-MnO_2 nanowires (Table 2, Appendix A in Supporting Information).

Table 3
Fitting of the O1s XPS spectra showing O bond type. Fitting adapted from literature [12,25,26].

Sample	O1s[a]		
	Bond type	BE (eV)	Area %
Pristine α-MnO_2	Mn—O—Mn	529.2	70.1
	Mn—OH	531.0	23.5
	H—O—H	532.3	6.4
72 h AL α-MnO_2	Mn—O—Mn	529.4	61.6
	Mn—OH	530.8	31.2
	H—O—H	531.8	7.2
Co doped AL α-MnO_2	Mn—O—Mn	529.5	55.7
	Mn—OH	530.7	37.0
	H—O—H	532.2	7.3
Co doped 72 h AL α-MnO_2	Mn—O—Mn	529.3	58.1
	Mn—OH	530.8	35.1
	H—O—H	531.8	6.7

The chemical characterization of acid-leached α-MnO_2 begins with the same AAS/IT approach as used for pristine α-MnO_2. However, it also incorporates two proposed theories of the mechanism of acid leaching, specifically the H^+–K^+ ion exchange mechanism [16] and the Mn^{3+} disproportionation mechanism [17,18,23]. In short, the ion exchange mechanism states that upon subjection to a strong acid, like HNO_3, K^+ stabilizing ions are extracted from α-MnO_2 structural tunnels. In response, the loss of cationic charge is compensated by the introduced protons from the acidic solution. On the other hand, the disproportionation mechanism proposes

that the presence of a strong acid causes two neighboring Mn^{3+} ions to exchange electrons resulting in one Mn^{2+} and one Mn^{4+} ion. Mn^{2+} ions are soluble in aqueous solutions and therefore have a driving force to leave the crystal structure. The leaving Mn^{2+} ions are believed to be accompanied by O^{2-} ions, thus increasing the average oxidation state (AOS) of manganese in remaining solid material in order to maintain charge balance. In both cases, acid-leaching is said to modify multiple sublattices of the α-MnO_2 crystal system producing a defect-rich material. Current discussion of these two mechanisms has revolved around the determination of which mechanism is dominant [18]. In our analysis, we found that each mechanism alone does not fully capture the entirety of the acid-leaching process and our experimental findings can only be explained by both of these mechanisms complimenting each other.

The dissolution of manganese due to the disproportionation of Mn^{3+} from the structural tunnel walls into Mn^{4+}, staying in structure of the solid material, and Mn^{2+}, dissolving in aqueous acidic environment [23], occurs according to the mechanism shown in Eq. (8):

$$2Mn^{3+} \rightarrow Mn^{2+} + Mn^{4+} \quad (8)$$

AAS measurements revealed the loss of 10.2% of Mn after acid leaching, which was confirmed by measuring the Mn content in the acid solution used during the acid-leaching process (Supporting Information, Table S3). Iodometric titration showed that the average oxidation state of Mn increased from +3.774 in pristine material to +3.966 in the acid-leached nanowires (Table 2). According to the Eq. (8), a loss of 10.2% of Mn coincides with the formation of an additional 10.2% of Mn^{4+} for an overall loss of 20.4% of Mn^{3+}. For example, if a pristine α-MnO_2 sample is comprised of 77 moles of Mn^{4+} and 23 moles of Mn^{3+}, and this dissolution mechanism occurs, then the sample would have 87.2 moles of Mn^{4+} and only 2.6 moles of Mn^{3+} after completion of the acid leaching process (Appendix A in Supporting Information). Subsequently, the α value, the ratio of Mn^{4+} to total Mn (Eq. (7)), of this theoretical sample would be 0.971. The experimental α value of 0.966 obtained from the titration of acid-leached material is in good agreement with this value confirming the validity of this combined AAS/IT method. This experimental approach agrees well with the theoretical mass balance calculations and yields a chemical composition for the acid-leached α-MnO_2 nanowires as $K_{0.03}Mn_{0.90}O_{1.86}$. While the charges in this formula are not balanced, the K^+-H^+ ion exchange mechanism may allow for the introduction of protons from the acidic solution to rectify this, resulting in the formula $H^+_{0.12}K^+_{0.03}Mn^{3.97+}_{0.90}O^{2-}_{1.86}$ (Table 2). Precedent for the introduction of H^+ ions exists in the widely discussed K^+–H^+ exchange mechanism that has been proposed to explain how K^+ stabilizing ions are removed from the α-MnO_2 crystal lattice during acid leaching [17,24] as discussed above. In our experiments, the amount of H^+ ions added to the chemical formula of the acid-leached material for the charge balance, matches well the loss of K^+ ions measured by AAS (Appendix A in Supporting Information). In the previous study [19] it was found that the protons incorporated into the structure of tunnel manganese oxide reside in the form of hydroxyl groups by attaching to the oxygen atoms in the inner walls of the structural tunnels. Therefore, an alternative way to write down a chemical formula of the acid-leached α-MnO_2 nanowires is: $K_{0.03}Mn_{0.90}O_{1.73}(OH)_{0.13}$. The increased fraction of hydroxyl groups in the acid-leached material is in agreement with the XPS measurements discussed below. Our findings suggest that two mechanisms of interaction between manganese oxides and strong oxidizing acids, ion exchange and Mn^{3+} disproportionation, are linked and occur simultaneously. This insight further highlights how a simple chemical treatment, like acid-leaching, has widespread effects on material structure and composition.

By combining the manganese dissolution theory and our AAS/IT study, we determined chemical formulas of pristine and acid-leached α-MnO_2 nanowires (Table 1) and proposed the following chemical reaction occurring after 72 h of acid leaching (Eq. (9)):

$$0.32HNO_{3\ (aq)} + K_{0.15}MnO_{1.96\ (s)} \rightarrow H_{0.12}K_{0.03}Mn_{0.90}O_{1.86\ (s)} + 0.12KNO_{3\ (aq)} + 0.10Mn(NO_3)_{2\ (aq)} + 0.10H_2O_{(l)} \quad (9)$$

Acid leaching also changes the composition of oxygen bonds on the surface of the material by increasing the proportion of Mn–OH to Mn–O–Mn bonds. Analysis of the O1s XPS spectra (Fig. 4c) indicates a decrease in the Mn–O–Mn bonds and an increase in Mn–OH bonds, as revealed by deconvolution of the O1s spectra and measurement of the surface area that corresponds to each individual bond (Table 3). We hypothesized that because each Mn ion is bonded to 6 oxygen atoms, in acidic media, the remaining oxygen atoms will form hydroxyl bonds to compensate for the removal of one Mn, in agreement with the previously stated hypothesis of the introduction of protons during acid leaching. Additionally, TGA/MS

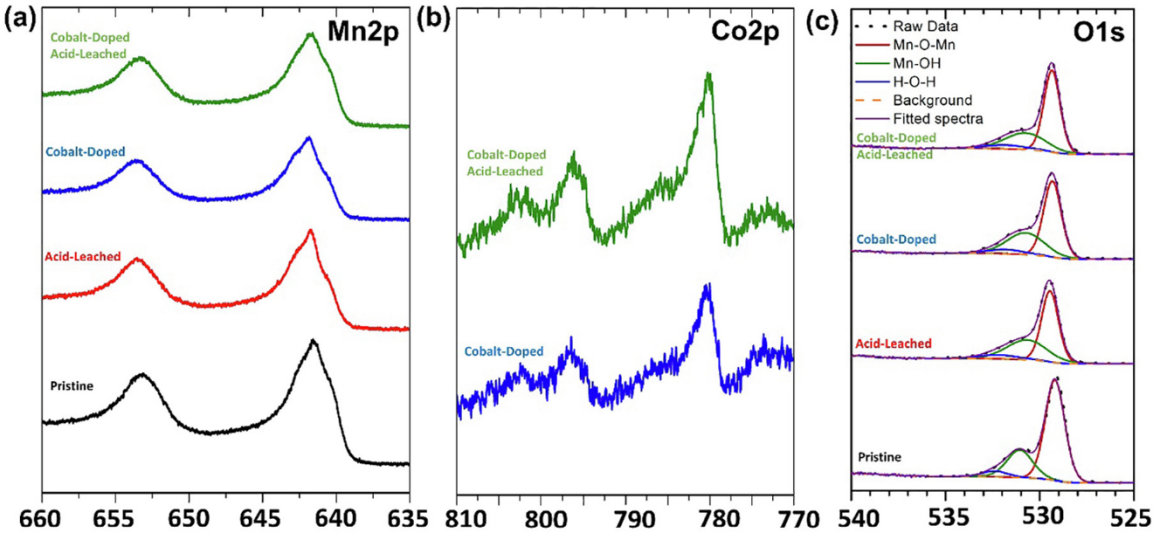

Fig. 4. (a) Mn 2p, (b) Co 2p, and (c) O 1s XPS spectra of the pristine and chemically modified α-MnO_2 nanowires.

data shows that defect rich acid-leached sample released hydroxyl groups upon heating not seen in the pristine sample (Supporting Information, Fig. S1), confirming the XPS findings of a higher occurrence of Mn–OH bonding after acid leaching. It should be noted that XPS is a surface only characterization technique, and it is expected that the amount of Mn–OH bonds would be slightly greater on the surface of the material then in the bulk, as Mn closer to the surface could more readily disproportionate and leave the crystal lattice.

Importantly, our combined ASS/IT characterization approach presents for the first time an efficient method to evaluate the fraction of oxygen vacancies in manganese oxides. This methodology can be exceptionally important to understand electrocatalytic and other properties of a large family of low-cost and environmentally friendly manganese oxides. Here we for the first time directly show that the crystal structure of the pristine α-MnO_2 nanowires has a small fraction of oxygen defects, resulting in a chemical formula of $K_{0.15}MnO_{1.96}$. This finding is important for multiple intercalation-based applications of this material, such as battery electrodes [11,12,18,27–29] and hybrid capacitive water desalination electrodes [30,31]. Oxygen vacancies have been shown to provide pathways for intertunnel ions diffusion [28], leading to improved rate performance of tunnel manganese oxide electrodes. Therefore, acid leaching can be used as an efficient mechanism to control the fraction of oxygen vacancies in manganese oxides. By tuning the nature of the acid as well as the time and temperature of interaction between the acid and manganese oxide, the manganese disproportionation process accompanied by the formation of oxygen vacancies can be regulated. However, it is important to note that our combined AAS/IT measurements approach does not efficiently account for the presence of hydroxyl groups, typically residing on the surface of manganese oxides, which can contribute to the change in the oxidation state of manganese in case of high surface area materials. A systematic study is needed to fully understand the limits and opportunities of the acid leaching of manganese oxides and establish correlations between acid leaching conditions, materials structure and properties.

3.3. Characterization of cobalt in Co-doped samples

SEM images and XRD patterns showed that the α-MnO_2 crystal structure was preserved in case of both pristine and acid-leached materials after cobalt doping (Fig. S2 in Supporting Information). SEM imaged did not show evidence of a secondary phase with morphology different from one-dimensional particles. Ma et al., reported that in-situ doping of α-MnO_2 with cobalt introduced Co^{3+} ions into the Mn sublattice [32]. In our work, satellite peaks indicative of Co^{2+} were clearly identified on the Co2p XPS spectra of all cobalt containing samples at binding energies of ~803 eV [25] and ~787 eV [33], (Fig. 4b). Unlike Co^{3+}, high spin Co^{2+} exists in a tetrahedral coordination and therefore it is unlikely to replace manganese in MnO_6 octahedra in tunnel walls [32,33].

The Mn2p (Fig. 4a) and Mn3p (Fig. S5 in Supporting Information) XPS spectra confirm that manganese is present in a mixed $Mn^{3+/4+}$ oxidation state in the structure of all materials investigated in this work. Analysis of the Mn3p XPS spectra according to the method proposed in work by Ilton et al. [34] revealed lowering of the oxidation state of Mn in Co-doped samples. Compositionally, doping pristine α-MnO_2 reduces the potassium atomic percent to 3.6% in all cases (Tables 1 and 2). Cobalt doping also caused the unit cell parameter *a* of the acid-leached α-MnO_2 to return to 9.849 Å (Table S2 in Supporting Information), suggesting that during the doping process there may be a degree of potassium-cobalt exchange and that cobalt resides in the structural tunnels of α-MnO_2. Moreover, when Co^{2+} has been introduced into layered manganese oxide phases, Co^{2+} was found to reside in the interlayer spacing of the MnO_2 layers and not in the Mn sublattice [14]. Therefore, our analyses indicate that cobalt ions are accommodated inside the structural tunnels after the cobalt doping achieved via interaction of manganese oxide nanowires with cobalt nitrate melt.

3.4. Electrochemical performance

Linear sweep voltammetry (LSV) was used to test the OER catalytic activity of pristine and chemically modified α-MnO_2 nanowires (Fig. 5a and b). Electrochemical performance of the materials investigated in this work is summarized in Table S4 in Supplementary Information. Pristine α-MnO_2 nanowires exhibited an ultimate current density of 21.6 mA·cm^{-2} at 1.85 V vs RHE and an overpotential of 564 mV at a current density of 10 mA·cm^{-2}, and a Tafel slope of 109 mV·dec^{-1} (Fig. 5). For reference, the OER activity of the electrode prepared without adding any active material was evaluated (Supporting Information, Fig. S3), confirming that α-MnO_2 nanowires serve as efficient electrocatalyst towards oxygen evolution in electrochemical water splitting.

The acid-leached nanowires exhibited a 30% increase in ultimate current densities and a reduction in overpotential at 10 mA·cm^{-2} to 516 mV (Table S4 in Supporting Information). This increase was attributed in part to creation of an irregular surface topology due to the partial dissolution of manganese and formation of oxygen vacancies. In the α-MnO_2 crystal system, each oxy-

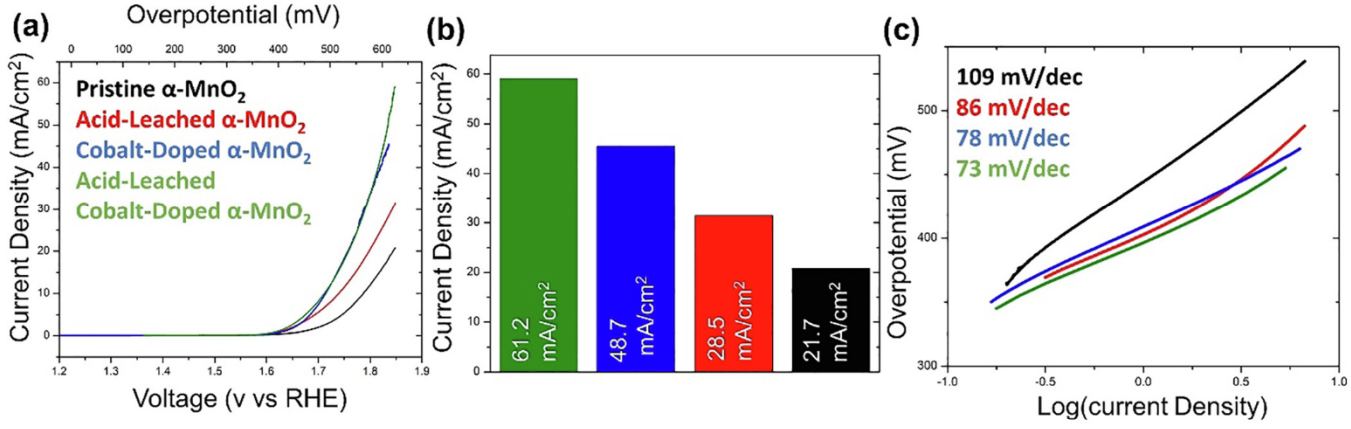

Fig. 5. Electrocatalytic performance of the pristine and chemically-modified α-MnO_2 nanowires. (a) Linear sweep voltammograms, (b) ultimate current density and (c) Tafel plots for OER on various electrocatalysts tested.

gen is bonded to three adjacent manganese atoms. The removal of one oxygen and one Mn ion would expose two additional manganese atoms that may not have been able to participate in catalysis before acid leaching. This is reflected in the molar mass lowering considerably as a result of acid leaching, meaning that more Mn per electrode is exposed to water than in case of the pristine material. Additionally, acid-leaching reduces the electronic resistivity of the material by a factor of three (Table S4 in Supporting Information) leading to improved electron transport. Acid leaching also reduced the Tafel slope of α-MnO_2 nanowires from 109 mV·dec^{-1} to 86 mV·dec^{-1}. This reduction in Tafel slope below 90 indicated that the rate-limiting steps in OER mechanism can be different in case of pristine and acid-leached α-MnO_2 electrocatalysts. This again can be caused by increase in the amount of Mn active sites and improved electronic conductivity (Table S4 in Supporting Information) resulting in superior catalytic performance of the acid-leached α-MnO_2 nanowires over pristine nanowires.

Cobalt doping was also shown to be a powerful method to increase OER catalytic activity of α-MnO_2 nanowires. The addition of cobalt (0.04 at%) more than doubled the ultimate current density in LSV experiments and lowered the Tafel slope to 78 mV·dec^{-1} (Fig. 5c, Table S4 in Supporting Information). This observation is in agreement with Grimaud et al.'s finding that high spin Co^{2+} ions serve as the most active cobalt species towards OER in perovskite crystal systems [35]. However, since our analyses revealed that Co^{2+} dopant ions reside within the structural tunnels of the α-MnO_2 and not in the Mn sublattice, it is unlikely that Co^{2+} significantly participate as additional active sites in OER catalysis. The size of the structural tunnels of α-MnO_2 phase is on the order of 4–5 Å making it unlikely that hydroxyl ions can diffuse through the tunnels, because hydrated hydroxyl ions can be as large as 6 Å [36]. Therefore, it is believed that the additional Co^{2+} ions improve OER activity by reducing the average oxidation state of Mn closer to 3.5 (Fig. 4) which is more favorable towards catalytic activity [2]. Thenuwara et al, have reported similar phenomenon in cobalt doped layer manganese oxides [14].

Cobalt doping of acid-leached α-MnO_2 nanowires combined the low Tafel slope of cobalt-doped nanowires (73 mV·dec^{-1}, Fig. 5 and Table S4 in Supporting Information) and the low electronic resistivity of acid-leached nanowires producing the material with the best OER performance. At voltages above 1.8 V vs RHE, the cobalt-doped pristine α-MnO_2 nanowires transitioned from an exponential to a linear behavior (Fig. 5a) indicating that this material is beginning to be impeded by a lack of electrons. The acid-leached and cobalt-doped material, however, exhibited exponential behavior at voltages above 1.8 V vs RHE, which allows it to achieve a higher ultimate current density. This phenomenon also highlights how acid leaching and cobalt doping are believed to influence OER activity in different ways: acid leaching exposes more Mn to act as active sites and increases the electronic conductivity of the nanowires, while cobalt doping introduces other electrochemically active Co^{2+} ions that may act as additional active sites for catalysis while enhancing existing Mn active sites by reducing the oxidation state of Mn closer to the theoretically ideal value of +3.5. In addition, cobalt doping can increase the conductivity in the *a-b* plane of α-MnO_2 structure, in agreement with the resistivity measurement shown in Table S4 in Supporting Information, thus further increasing catalytic activity. Together these chemical modification approaches modified the structure and chemical composition of α-MnO_2 nanowires to increase ultimate current densities by over 300% and reduce the overpotential by over 70 mV compared to the pristine material (Fig. 5 and Table S4) producing an electrocatalyst with superior performance. Chronoamperometry measurements revealed that the cobalt-doped acid-leached material's electrochemical stability is on par with that of the other materials suggesting that the creation of a defect rich manganese oxide does not greatly affect catalytic reliability (Fig. S4 in Supporting Information). The chemical modification approaches, developed in this work, can be adapted to other polymorphs of manganese oxide and/or be used in conjunction with advance electrode architectures through electrocatalytically active metal nanoparticle decoration.

4. Conclusions

In this work, the post synthesis chemical modification approaches of acid leaching and cobalt doping have been shown to be powerful strategies to enhance the OER activity of α-MnO_2 nanowires. Acid leaching was used to modify the anionic sublattice, and we determined a 5.1% increase in the fraction of oxygen vacancies in α-MnO_2 nanowires after 72 h of interaction with concentrated nitric acid at room temperature. The enhanced electrocatalytic performance shown by the acid-leached α-MnO_2 nanowires was attributed to exposure of additional Mn active sites and increased electronic conductivity of the oxygen-deficient material. Cobalt doping introduced Co^{2+} ions into the structural tunnels of the α-MnO_2 nanowires that are believed to improve the OER activity by lowering the average oxidation state of Mn closer to +3.5, the theoretically predicted ideal value for OER activity, and may serve as additional OER active sites. This is reinforced by cobalt doping lowering the Tafel slope below 80 mV·dec^{-1} and more than doubling the ultimate current densities. When used in tandem, the high activity of the cobalt-doped α-MnO_2 nanowires was combined with the improved electronic conductivity and exposed active sites of the acid-leached α-MnO_2 nanowires producing a superior electrocatalyst with more than a 3-fold increase in OER activity over pristine material. Moreover, these chemical treatments did not affect the longevity of reliability of the electrocatalysts. The chemical modification methods explored in this work highlight the diverse approaches that can be taken to improve the catalytic activity of manganese oxides by creating defect-rich materials with enhanced performance in oxygen evolution reaction. Once the limiting factor of a catalyst system is identified, the correct post synthesis treatment could be applied to improve the system. Moreover, the facile and scalable nature of these post synthesis treatments suggests that they can readily be applied to other classes of materials.

Acknowledgements

The authors of this work would like to acknowledge financial support from National Science Foundation, USA (grant CMMI-1635233). We thank Drexel's Centralized Research Facilities, Mallory Clites, Brendan Hayes-Oberst, Dr. Babak Anasori, and Dr. Mykola Seredych for their help with materials characterization and Prof. Maureen Tang for her insights on electrocatalysis.

Appendix A. Supplementary data

Supplementary data to this article can be found online at https://doi.org/10.1016/j.poly.2019.06.050.

References

[1] A. Godula-Jopek, D. Stolten, Hydrogen Production: By Electrolysis, John Wiley & Sons, Incorporated, Berlin, Germany, 2015.
[2] N.-T. Suen, S.-F. Hung, Q. Quan, N. Zhang, Y.-J. Xu, H.M. Chen, Electrocatalysis for the oxygen evolution reaction: recent development and future perspectives, Chem. Soc. Rev. 46 (2) (2017) 337.
[3] E. Antolini, Iridium as catalyst and cocatalyst for oxygen evolution/reduction in acidic polymer electrolyte membrane electrolyzers and fuel cells, ACS Catal. 4 (5) (2014) 1426.

[4] Y. Cheng, S.P. Jiang, Advances in electrocatalysts for oxygen evolution reaction of water electrolysis-from metal oxides to carbon nanotubes, Progr. Nat. Sci.: Mater. Int. 25 (6) (2015) 545.

[5] R. Subbaraman, D. Tripkovic, K.-C. Chang, D. Strmcnik, A.P. Paulikas, P. Hirunsit, M. Chan, J. Greeley, V. Stamenkovic, N.M. Markovic, Trends in activity for the water electrolyser reactions on 3d M(Ni Co, Fe, Mn) hydr(oxy)oxide catalysts, Nat Mater 11 (6) (2012) 550.

[6] A. Eftekhari, Tuning the electrocatalysts for oxygen evolution reaction, Mater. Today Energy 5 (2017) 37.

[7] X.-F. Luo, J. Wang, Z.-S. Liang, S.-Z. Chen, Z.-L. Liu, C.-W. Xu, Manganese oxide with different morphology as efficient electrocatalyst for oxygen evolution reaction, Int. J. Hydrogen Energy 42 (10) (2017) 7151.

[8] R. Pokhrel, M.K. Goetz, S.E. Shaner, X. Wu, S.S. Stahl, The "best catalyst" for water oxidation depends on the oxidation method employed: a case study of manganese oxides, JACS 137 (26) (2015) 8384.

[9] A. Iyer, J. Del-Pilar, C.K. King'ondu, E. Kissel, H.F. Garces, H. Huang, A.M. El-Sawy, P.K. Dutta, S.L. Suib, Water oxidation catalysis using amorphous manganese oxides, octahedral molecular sieves (OMS-2), and octahedral layered (OL-1) manganese oxide structures, J. Phys. Chem. C 116 (10) (2012) 6474.

[10] Y. Meng, W. Song, H. Huang, Z. Ren, S.-Y. Chen, S.L. Suib, Structure-property relationship of bifunctional MnO_2 nanostructures: highly efficient, ultra-stable electrochemical water oxidation and oxygen reduction reaction catalysts identified in alkaline media, JACS 136 (32) (2014) 11452.

[11] B.W. Byles, N.K.R. Palapati, A. Subramanian, E. Pomerantseva, The role of electronic and ionic conductivities in the rate performance of tunnel structured manganese oxides in Li-ion batteries, APL Mater. 4 (4) (2016) 046108.

[12] A.S. Poyraz, J. Huang, C.J. Pelliccione, X. Tong, S. Cheng, L. Wu, Y. Zhu, A.C. Marschilok, K.J. Takeuchi, E.S. Takeuchi, Synthesis of cryptomelane type α-MnO_2 ($K_xMn_8O_{16}$) cathode materials with tunable K^+ content: the role of tunnel cation concentration on electrochemistry, J. Mater. Chem. A 5 (32) (2017) 16914.

[13] C.-H. Kuo, W. Li, L. Pahalagedara, A.M. El-Sawy, D. Kriz, N. Genz, C. Guild, T. Ressler, S.L. Suib, J. He, Understanding the role of gold nanoparticles in enhancing the catalytic activity of manganese oxides in water oxidation reactions, Angew. Chem. Int., Ed. 54 (8) (2015) 2345.

[14] A.C. Thenuwara, S.L. Shumlas, N.H. Attanayake, Y.V. Aulin, I.G. McKendry, Q. Qiao, Y. Zhu, E. Borguet, M.J. Zdilla, D.R. Strongin, Intercalation of cobalt into the interlayer of birnessite improves oxygen evolution catalysis, ACS Catal. 6 (11) (2016) 7739.

[15] A.C. Thenuwara, E.B. Cerkez, S.L. Shumlas, N.H. Attanayake, I.G. McKendry, L. Frazer, E. Borguet, Q. Kang, R.C. Remsing, M.L. Klein, M.J. Zdilla, D.R. Strongin, Nickel confined in the interlayer region of birnessite: an active electrocatalyst for water oxidation, Angew. Chem. Int., Ed. 55 (35) (2016) 10381.

[16] J.-H. Lee, R. Black, G. Popov, E. Pomerantseva, F. Nan, G.A. Botton, L.F. Nazar, The role of vacancies and defects in $Na_{0.44}MnO_2$ nanowire catalysts for lithium-oxygen batteries, Energy Environ. Sci. 5 (11) (2012) 9558.

[17] B. Byles, A. Subramanian, E. Pomerantseva, in: Acid-leached α-MnO2 nanowires for electrochemical energy storage, SPIE NanoScience + Engineering, SPIE: 2014; p 8.

[18] Y. Yuan, C. Zhan, K. He, H. Chen, W. Yao, S. Sharifi-Asl, B. Song, Z. Yang, A. Nie, X. Luo, H. Wang, S.M. Wood, K. Amine, M.S. Islam, J. Lu, R. Shahbazian-Yassar, The influence of large cations on the electrochemical properties of tunnel-structured metal oxides, Nat. Commun. 7 (2016) 13374.

[19] E.A. Pomerantseva, L.S. Leonova, E.A. Goodilin, Y.A. Dobrovolsky, Y.D. Tretyakov, Proton conduction of $Ba_6Mn_{24}O_{48}$ tunnel manganite, Solid State Ionics 180 (2) (2009) 187.

[20] Y. Gao, Z. Wang, J. Wan, G. Zou, Y. Qian, A facile route to synthesize uniform single-crystalline α-MnO_2 nanowires, J. Cryst. Growth 279 (3) (2005) 415.

[21] R. Laiho, K.G. Lisunov, E. Lähderanta, P.A. Petrenko, J. Salminen, V.N. Stamov, Y. P. Stepanov, V.S. Zakhvalinskii, Low-field magnetic properties of $LaMnO_{3+\delta}$ with $0.065 \leq \delta \leq 0.154$, J. Phys. Chem. Solids 64 (12) (2003) 2313.

[22] C. Vazquez-Vazquez, M. Carmen Blanco, M. Arturo Lopez-quintela, R. Sanchez, J. Rivas, B. Oseroff, S„ Characterization of $La_{0.67}Ca_{0.33}MnO_{3+/-\delta}$ particles prepared by the sol-gel route, J. Mater. Chem. 8 (4) (1998) 991.

[23] F. Pagnanelli, G. Furlani, P. Valentini, F. Vegliò, L. Toro, Leaching of low-grade manganese ores by using nitric acid and glucose: optimization of the operating conditions, Hydrometallurgy 75 (1) (2004) 157.

[24] Y. Tanaka, M. Tsuji, Y. Tamaura, ESCA and thermodynamic studies of alkali metal ion exchange reactions on an α-MnO_2 phase with the tunnel structure, PCCP 2 (7) (2000) 1473.

[25] M.C. Biesinger, B.P. Payne, A.P. Grosvenor, L.W.M. Lau, A.R. Gerson, R.S.C. Smart, Resolving surface chemical states in XPS analysis of first row transition metals, oxides and hydroxides: Cr, Mn, Fe, Co and Ni, Applied Surface Science 257 (7) (2011) 2717.

[26] M. Toupin, T. Brousse, D. Bélanger, Charge storage mechanism of MnO_2 electrode used in aqueous electrochemical capacitor, Chem. Mater. 16 (16) (2004) 3184.

[27] B.W. Byles, P. West, D.A. Cullen, K.L. More, E. Pomerantseva, Todorokite-type manganese oxide nanowires as an intercalation cathode for Li-ion and Na-ion batteries, RSC Adv. 5 (128) (2015) 106265.

[28] L. Wu, F. Xu, Y. Zhu, A.B. Brady, J. Huang, J.L. Durham, E. Dooryhee, A.C. Marschilok, E.S. Takeuchi, K.J. Takeuchi, Structural defects of silver hollandite, $Ag_xMn_8O_y$, nanorods: dramatic impact on electrochemistry, ACS Nano 9 (8) (2015) 8430.

[29] Y. Yuan, C. Liu, B.W. Byles, W. Yao, B. Song, M. Cheng, Z. Huang, K. Amine, E. Pomerantseva, R. Shahbazian-Yassar, J. Lu, Ordering heterogeneity of [MnO_6] octahedra in tunnel-structured MnO_2 and its influence on ion storage, Joule 3 (2) (2019) 471.

[30] L. Agartan, B. Hayes-Oberst, B.W. Byles, B. Akuzum, E. Pomerantseva, E. Caglan Kumbur, Influence of operating conditions and cathode parameters on desalination performance of hybrid CDI systems, Desalination 452 (2019) 1.

[31] B.W. Byles, D.A. Cullen, K.L. More, E. Pomerantseva, Tunnel structured manganese oxide nanowires as redox active electrodes for hybrid capacitive deionization, Nano Energy 44 (2018) 476.

[32] J. Ma, C. Wang, H. He, Transition metal doped cryptomelane-type manganese oxide catalysts for ozone decomposition, Appl. Catal. B 201 (2017) 503.

[33] R. Tholkappiyan, K. Vishista, Tuning the composition and magnetostructure of dysprosium iron garnets by Co-substitution: An XRD, FT-IR, XPS and VSM study, Appl. Surf. Sci. 351 (2015) 1016.

[34] E.S. Ilton, J.E. Post, P.J. Heaney, F.T. Ling, S.N. Kerisit, XPS determination of Mn oxidation states in Mn (hydr)oxides, Appl. Surf. Sci. 366 (2016) 475.

[35] A. Grimaud, C.E. Carlton, M. Risch, W.T. Hong, K.J. May, Y. Shao-Horn, Oxygen evolution activity and stability of $Ba_6Mn_5O_{16}$, $Sr_4Mn_2CoO_9$, and $Sr_6Co_5O_{15}$: the influence of transition metal coordination, J. Phys. Chem. C 117 (49) (2013) 25926.

[36] D. Asthagiri, L.R. Pratt, J.D. Kress, M.A. Gomez, The hydration state of HO^-(aq), Chem. Phys. Lett. 380 (5) (2003) 530.